# Dipole limit in second-harmonic generation from arrays of gold nanoparticles

**Robert Czaplicki,[1,*] Mariusz Zdanowicz,[1,2] Kalle Koskinen,[1] Janne Laukkanen,[3] Markku Kuittinen,[3] and Martti Kauranen[1]**

[1]*Department of Physics, Tampere University of Technology, P.O. Box 692, FI-33101 Tampere, Finland*
[2]*National Institute of Telecommunications, Szachowa 1, PL-04894 Warsaw, Poland*
[3]*Department of Physics and Mathematics, University of Eastern Finland, FI-80101 Joensuu, Finland*
[*]*robert.czaplicki@tut.fi*

**Abstract:** We present a multipolar tensor analysis of second-harmonic generation from arrays of noncentrosymmetric gold nanoparticles. In contrast to earlier results, where higher multipoles and symmetry-forbidden signals arising from sample defects play a significant role, the present results are completely dominated by symmetry-allowed electric-dipole tensor components. The result arises from significant improvement in sample quality, which suppresses the higher-multipole effects and enhances the overall response by an order of magnitude. The results are a prerequisite for metamaterials with controllable nonlinear properties.



**OCIS codes:** (190.0190) Nonlinear optics; (310.6628) Subwavelength structures, nanostructures; (160.4236) Nanomaterials; (160.3900) Metals.

## References and links

1. V. M. Shalaev, "Optical negative-index metamaterials," Nat. Photonics **1**(1), 41–48 (2007).
2. U. Kreibig and M. Vollmer, *Optical Properties of Metal Clusters*, Springer Series in Materials Science (Springer, New York, 1995).
3. K. L. Kelly, E. Coronado, L. L. Zhao, and G. C. Schatz, "The optical properties of metal nanoparticles: The influence of size, shape, and dielectric environment," J. Phys. Chem. B **107**(3), 668–677 (2003).
4. W. Cai, U. K. Chettiar, A. V. Kildishev, and V. M. Shalaev, "Optical cloaking with metamaterials," Nat. Photonics **1**(4), 224–227 (2007).
5. T. Ergin, N. Stenger, P. Brenner, J. B. Pendry, and M. Wegener, "Three-dimensional invisibility cloak at optical wavelengths," Science **328**(5976), 337–339 (2010).
6. B. K. Canfield, H. Husu, J. Laukkanen, B. Bai, M. Kuittinen, J. Turunen, and M. Kauranen, "Local field asymmetry drives second-harmonic generation in non-centrosymmetric nanodimers," Nano Lett. **7**(5), 1251–1255 (2007).
7. M. W. Klein, M. Wegener, N. Feth, and S. Linden, "Experiments on second- and third-harmonic generation from magnetic metamaterials," Opt. Express **15**(8), 5238–5247 (2007).
8. F. B. P. Niesler, N. Feth, S. Linden, and M. Wegener, "Second-harmonic optical spectroscopy on split-ring-resonator arrays," Opt. Lett. **36**(9), 1533–1535 (2011).
9. B. K. Canfield, S. Kujala, K. Jefimovs, T. Vallius, J. Turunen, and M. Kauranen, "Polarization effects in the linear and nonlinear optical responses of gold nanoparticle arrays," J. Opt. A Pure Appl Opt. **7**(2), S110–S117 (2005).
10. B. K. Canfield, S. Kujala, K. Jefimovs, J. Turunen, and M. Kauranen, "Linear and nonlinear optical responses influenced by broken symmetry in an array of gold nanoparticles," Opt. Express **12**(22), 5418–5423 (2004).
11. J. A. H. van Nieuwstadt, M. Sandtke, R. H. Harmsen, F. B. Segerink, J. C. Prangsma, S. Enoch, and L. Kuipers, "Strong modification of the nonlinear optical response of metallic subwavelength hole arrays," Phys. Rev. Lett. **97**(14), 146102 (2006).
12. M. W. Klein, Ch. Enkrich, M. Wegener, and S. Linden, "Second-harmonic generation from magnetic metamaterials," Science **313**(5786), 502–504 (2006).
13. M. Gentile, M. Hentschel, R. Taubert, H. Guo, H. Giessen, and M. Fiebig, "Investigation of the nonlinear optical properties of metamaterials by second harmonic generation," Appl. Phys. B **105**(1), 149–162 (2011).
14. S. Kujala, B. K. Canfield, M. Kauranen, Y. Svirko, and J. Turunen, "Multipolar analysis of second-harmonic radiation from gold nanoparticles," Opt. Express **16**(22), 17196–17208 (2008).
15. M. I. Stockman, D. J. Bergman, C. Anceau, S. Brasselet, and J. Zyss, "Enhanced second-harmonic generation by metal surfaces with nanoscale roughness: nanoscale dephasing, depolarization, and correlations," Phys. Rev. Lett. **92**(5), 057402 (2004).
16. M. I. Stockman, "Nanoscience: Dark-hot resonances," Nature **467**(7315), 541–542 (2010).

#157528 - $15.00 USD Received 2 Nov 2011; revised 7 Dec 2011; accepted 7 Dec 2011; published 15 Dec 2011

17. M. Zdanowicz, S. Kujala, H. Husu, and M. Kauranen, "Effective medium multipolar tensor analysis of second harmonic generation from metal nanoparticles," New J. Phys. **13**(2), 023025 (2011).
18. J. Nappa, G. Revillod, I. Russier-Antoine, E. Benichou, C. Jonin, and P.-F. Brevet, "Electric dipole origin of the second harmonic generation of small metallic particles," Phys. Rev. B **71**(16), 165407 (2005).
19. J. Butet, G. Bachelier, I. Russier-Antoine, C. Jonin, E. Benichou, and P.-F. Brevet, "Interference between selected dipoles and octupoles in the optical second-harmonic generation from spherical gold nanoparticles," Phys. Rev. Lett. **105**(7), 077401 (2010).
20. J. I. Dadap, J. Shan, K. B. Eisenthal, and T. F. Heinz, "Second-harmonic rayleigh scattering from a sphere of centrosymmetric material," Phys. Rev. Lett. **83**(20), 4045–4048 (1999).
21. S. Roke, M. Bonn, and A. V. Petukhov, "Nonlinear optical scattering: The concept of effective susceptibility," Phys. Rev. B **70**(11), 115106 (2004).
22. A. G. F. de Beer, S. Roke, and J. I. Dadap, "Theory of optical second-harmonic and sum-frequency scattering from arbitrarily shaped particles," J. Opt. Soc. Am. B **28**(6), 1374–1384 (2011).
23. H. Husu, J. Mäkitalo, J. Laukkanen, M. Kuittinen, and M. Kauranen, "Particle plasmon resonances in L-shaped gold nanoparticles," Opt. Express **18**(16), 16601–16606 (2010).
24. B. K. Canfield, S. Kujala, K. Jefimovs, Y. Svirko, J. Turunen, and M. Kauranen, "A macroscopic formalism to describe the second-order nonlinear optical response of nanostructures," J. Opt. A Pure Appl. Opt. **8**(4), S278–S284 (2006).
25. M. Kauranen, T. Verbiest, and A. Persoons, "Second-order nonlinear optical signatures of surface chirality," J. Mod. Opt. **45**(2), 403–423 (1998).
26. S. Kujala, B. K. Canfield, M. Kauranen, Y. Svirko, and J. Turunen, "Multipole interference in the second-harmonic optical radiation from gold nanoparticles," Phys. Rev. Lett. **98**(16), 167403 (2007).

Metamaterials are artificial nanostructures whose optical properties arise from the geometry of their structural features [1]. Such materials often consist of arrays of metal nanoparticles whose optical properties are dominated by the collective oscillations of the conduction electrons in the particles. The oscillations give rise to plasmonic and magnetic resonances, which depend on the size, shape, dielectric environment, and mutual ordering of the particles [2,3]. The resonances can lead to strong electromagnetic fields near the particles and thus enhance optical interactions. The linear optical responses tailored in such ways are utilized, e.g., to achieve negative index of refraction [1] or cloaking [4,5].

The local-field enhancement is particularly important for nonlinear optical processes, which scale with a high power of the field. For second-order effects, noncentrosymmetric structures are needed, and the response is also otherwise very sensitive to symmetry. Such structures have been characterized by second-harmonic generation (SHG) in order to understand the role of the structural features [6,7] and resonance enhancement [8,9] in the efficiency of SHG.

An important problem in these efforts has been that the selection rules between the allowed and forbidden SHG signals, as derived from the ideal structural symmetry, have not been fulfilled [10–13]. In some cases, forbidden signals have even dominated the response [14]. This problem arises from symmetry-breaking nanoscale defects of the structures. The defects can act as attractors for particularly strong local fields [15,16] and thus play a disproportionate role in the second-order response. Even when the local response of the defects is dipolar, they give rise to characteristic higher-multipole (magnetic-dipole and electric-quadrupole) features in SHG when analyzed using effective-medium concepts appropriate for metamaterials [14]. In the most detailed analysis to date, the tensor components associated with higher-multipole effects were up to 50% in magnitude compared to the dominant electric-dipole component [17]. Furthermore, the symmetry-forbidden signals were dominated by higher-multipole effects, thus emphasizing their connection to defects. It is evident that it is not acceptable to have random defects significantly influence the nonlinear response if one aims to develop nonlinear metamaterials with the response tailored by the structural features of the sample. Beyond results regarding multipole effects in coherent SHG, their role has also been addressed in incoherent hyper-Rayleigh scattering [18,19], described with different levels of detail from first-principles approaches [20] to effective quantities [21,22].

In this study, we show that the dipole limit of SHG can be reached by using nanostructured samples with significantly improved quality. We prepare an array of noncentrosymmetric gold nanoparticles and analyze its response in terms of effective electric-dipole and higher-multipole tensors. We show that the response is dominated by the

#157528 - $15.00 USD Received 2 Nov 2011; revised 7 Dec 2011; accepted 7 Dec 2011; published 15 Dec 2011

symmetry-allowed electric-dipole tensor components. The higher-multipole tensor components are found to be at most a few percent of the dominant dipolar component and for most cases well below this. In addition, the nonlinear response is enhanced by a factor of 10 compared to samples of earlier generation with lower quality. We have thus essentially reached the dipole limit in SHG, implying that the response is dominated by the overall features of the sample, not by random defects. This is a prerequisite for tailoring the nonlinear response in a controllable way by the structural features of the sample.

Our sample consists of an array of L-shaped gold nanoparticles (Fig. 1(a)), prepared by electron-beam lithography and lift-off. The particle dimensions were chosen to yield a plasmonic resonance at the laser wavelength used for the SHG experiments (1060 nm). The nominal linewidth is 100 nm and both arms have the equal length of 250 nm. The thickness of the gold layer is 20 nm and there is a thin adhesion layer of chromium between the fused silica substrate and the gold. In addition, the sample was covered by a 20-nm thick protective layer of silica. The array period is 500 nm in both directions and the total sample area is 1 × 1 $mm^2$.

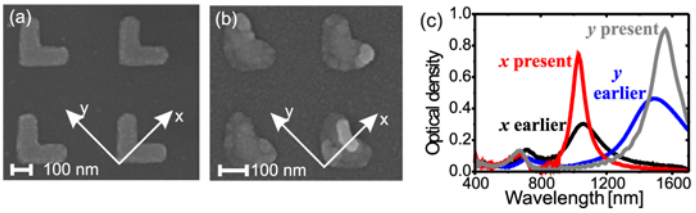


Fig. 1. SEM images and geometry of arrays of L-shaped nanoparticles for present, high-quality (a) and earlier, low-quality (b) samples. (c) *x*- and *y*-polarized extinction spectra of high- and low-quality samples.

For comparison, a sample from an earlier generation is also shown (Fig. 1(b)), where defects and higher multipole effects played a significant role in the SHG response [17]. The other main difference is that the array period of the old sample is 400 nm. It is evident from the SEM images of the quality of the present sample is significantly improved. The improvement is possible due to a new electron-beam lithography system, which has better accuracy and beam stability than the old system. The new system is also faster allowing smaller beam step size and thus improved line quality. Due to the high accelerating voltage (100 kV) of the new system, the forward scattering of electrons is smaller, which improves the shape control of the patterns further. Beyond the present sample, several others have been prepared with similar quality.

The samples are described using a coordinate system where *x* is the in-plane symmetry axis of the L shape and *y* is the orthogonal in-plane direction. The extinction spectra of the samples (Fig. 1(c)) were measured using fiber optic spectrometers at normal incidence. The samples are strongly dichroic with main resonances at similar wavelengths. The *x*-polarized resonances occur at 1033 nm (present sample) and 1060 nm (earlier sample) and the *y*-polarized resonances at 1554 nm (present) and 1490 nm (earlier). Additional resonances at 680 nm (present) and 710 nm (earlier) are related to the linewidth of the particles [23]. An important observation is that the extinction peak of the present sample is greatly enhanced and the linewidth narrowed. This is a direct consequence of the significantly improved sample quality with much less inhomogeneous broadening.

The nonlinear response is usually described by the nonlinear susceptibility tensor of the material. In nanostructures, however, the local fields and material properties exhibit nanoscale variations, which complicates such an approach. In order to avoid such nanoscale difficulties, we use the nonlinear response tensor (NRT) $A_{ijk}$ [24], which operates on the level of input and output radiation fields

$$E_i(2\omega) = \sum_{jk} A_{ijk} E_j(\omega) E_k(\omega), \qquad (1)$$

#157528 - $15.00 USD Received 2 Nov 2011; revised 7 Dec 2011; accepted 7 Dec 2011; published 15 Dec 2011

where *ijk* refer to the polarization components of the respective fields. NRT is strictly specific to a given experiment rather than the sample itself. Its benefit is that it includes all multipole effects implicitly and it allows the signals to be analyzed using electric-dipole symmetry rules. Within the effective medium approach, NRT is proportional to the effective susceptibility of the nanostructure. Furthermore, the NRT approach can be extended to account for effective electric-dipole and higher-multipole effects. Due to difficulties in separating magnetic and quadrupole effects from each other in coherent signals [25], both are included in effective magnetic tensors. This results in three effective tensors, which describe electric-dipole interactions only $\left(A_{ijk}^{eee}\right)$, magnetic interactions at the fundamental frequency $\left(A_{ijk}^{eem}\right)$, and magnetic interactions at the second-harmonic frequency $\left(A_{ijk}^{mee}\right)$ [17].

The three tensors can be separated from each other by comparing SHG signals in the transmitted (T) and reflected (R) directions and for metal (M) and substrate (S) side incidence of the fundamental field [17]. When the fundamental beam is normally incident on the sample along *z* direction, any SHG signal can always be expressed in the general form

$$E_i(2\omega) = fE_x^2(\omega) + gE_y^2(\omega) + hE_x(\omega)E_y(\omega), \qquad (2)$$

where the expansion coefficients *f*, *g*, and *h* depend on the components of the three tensors and are different for the various experimental geometries. For our present sample, which exhibits a resonance for *x*-polarized fundamental field, the SHG signal is expected to be dominated by its *x*-polarized component. The expansion coefficients for *x*-polarized detection and the various experimental geometries are shown in Table 1. It is evident that if only symmetry-allowed (*f* and *g*) and dipolar effects play a role, all four signals should behave in the same way. On the other hand, symmetry-forbidden and higher-multipole effects contribute with varying signs to different signals, making possible the determination of all tensor components.

**Table 1. The expansion coefficients expressed as function of NRT components for specific configurations. The signs depend on measurement geometry (M-: metal side incidence, S-: substrate side incidence, -T: transmission, -R: reflection). Note that *f* and *g* are allowed for the ideal symmetry of the L shape, whereas *h* is forbidden.**

| Geometry | *f* | *g* | *h* |
|---|---|---|---|
| M-T | $A_{xxx}^{eee} + A_{xxy}^{eem} + A_{yxx}^{mee}$ | $A_{xyy}^{eee} - A_{xyx}^{eem} + A_{yyy}^{mee}$ | $A_{xxy}^{eee} + (A_{xyy}^{eem} - A_{xxx}^{eem}) + A_{yxy}^{mee}$ |
| M-R | $A_{xxx}^{eee} + A_{xxy}^{eem} - A_{yxx}^{mee}$ | $A_{xyy}^{eee} - A_{xyx}^{eem} - A_{yyy}^{mee}$ | $A_{xxy}^{eee} + (A_{xyy}^{eem} - A_{xxx}^{eem}) - A_{yxy}^{mee}$ |
| S-T | $A_{xxx}^{eee} - A_{xxy}^{eem} - A_{yxx}^{mee}$ | $A_{xyy}^{eee} + A_{xyx}^{eem} - A_{yyy}^{mee}$ | $-A_{xxy}^{eee} + (A_{xyy}^{eem} - A_{xxx}^{eem}) + A_{yxy}^{mee}$ |
| S-R | $A_{xxx}^{eee} - A_{xxy}^{eem} + A_{yxx}^{mee}$ | $A_{xyy}^{eee} + A_{xyx}^{eem} + A_{yyy}^{mee}$ | $-A_{xxy}^{eee} + (A_{xyy}^{eem} - A_{xxx}^{eem}) - A_{yxy}^{mee}$ |

Our experimental setup for SHG is shown in Fig. 2. A Nd:glass laser (200 fs pulse length, 82 MHz repetition rate) provided the fundamental beam at 1060 nm and its average power before the sample was 80 mW. The beam was weakly focused with 300 mm focal length lens on the sample, resulting in spot size of 300 μm. The polarization of the beam was set to *x* or y direction and then continuously modulated with a quarter-wave plate (QWP). Any possible

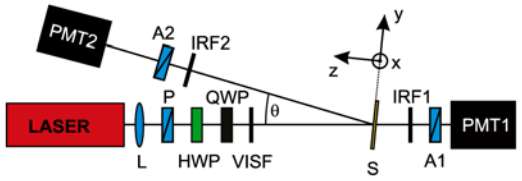


Fig. 2. Experimental setup. L – lens, P – polarizer, A1, A2 – analyzers, HWP – half-wave plate, QWP – quarter wave plate, VISF – visible blocking filter, IRF1, IRF2 – infrared blocking filters, PMT1, PMT2 – photomultiplier tubes.

#157528 - $15.00 USD Received 2 Nov 2011; revised 7 Dec 2011; accepted 7 Dec 2011; published 15 Dec 2011

SHG light from the optical components preceding the sample was filtered with a visible-blocking filter. The SHG signals were detected by photomultiplier tubes and photon counting by first filtering away the fundamental beam with infrared-blocking filters and using analyzers to pass only *x*-polarized SHG light.

The sample was slightly tilted off-normal with respect to fundamental beam ($\theta$ less than 2°) to allow detection of reflected SH radiation. The angle is sufficiently small that the fields do not couple significantly to the normal direction (*z*) of the sample [14,26].

The above measurements allow the relative complex values of the expansion coefficients to be determined for each signal separately. However, absolute calibration of the various signals is essentially impossible. The signals were thus separately normalized and their polarization lineshapes compared to obtain evidence of the presence or absence of higher multipole effects.

The measured signals (M-T, M-R, S-T and S-R) as functions of the rotation angle of the QWP and their fits to Eq. (2) are shown in Fig. 3. The lineshapes for S incidence have been reflected with respect to the zero angle of QWP to counter the sign change of the *y*-axis (*h* coefficient in Table 1) when the sample is flipped. All four signals should then show the same dependence on the polarization if only electric dipoles play role, whereas higher multipoles would lead to differences in the measured signals. All four measured lineshapes in Fig. 3 are seen to overlap almost perfectly. This result suggests that the SHG response of the present sample is strongly dominated by the electric-dipole interaction.

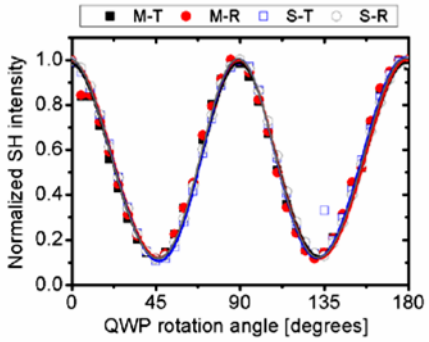


Fig. 3. Normalized transmitted (-T) and reflected (-R) SHG signals from an array of L-shaped gold nanoparticles for metal incidence (M-) and substrate incidence (S-), and from the present high-quality sample. Symbols represent the data from the measurements and solid lines are theoretical fits. The starting and detected linear polarization was *x*.

For more quantitative information about the various multipole effects, the fitted values of the coefficients *f*, *g* and *h* for the measured signals were compared to their expressions in terms of the components of the tensors (Table 1). This results in a group of linear equations, whose solution yields the relative complex values of the components (Table 2). The values are normalized to the dominant component $A_{xxx}^{eee}$, which has electric-dipole origin. $A_{xxx}^{eee}$ is allowed for the ideal structure and has a plasmonic resonance at the fundamental wavelength.

The response is clearly dominated by the allowed electric-dipole components $A_{xxx}^{eee}$ and $A_{xyy}^{eee}$, whereas the forbidden dipolar component $A_{xxy}^{eee}$ is very weak. In addition, the magnitudes of the components of the two magnetic tensors remain below 2% of the dominant component with the exception of the combination $\left(A_{xyy}^{eem} - A_{xxx}^{eem}\right)$ which is 3.5%. Interestingly, this component is symmetry-forbidden, i.e., it arises from the residual imperfections of the sample. Nevertheless the results are a significant improvement compared to those for the low-quality particles shown in Fig. 1(b), where the higher multipolar components had magnitudes up to 50% of the dominant dipolar components [17].

#157528 - $15.00 USD Received 2 Nov 2011; revised 7 Dec 2011; accepted 7 Dec 2011; published 15 Dec 2011

In order to exclude any other possibilities for higher-multipole effects, we also measured the *y*-polarized SHG signals. They were always found to be weaker than the *x*-polarized signals by an order of magnitude and also dominated by electric-dipole effects. These results will thus not change the general conclusion presented above. Improvements in the sample quality have thus allowed us to reach essentially the dipole limit in the SHG response.

**Table 2. Determined values of NRT components**

| Tensor component | Allowed | Value | Magnitude |
|---|---|---|---|
| $A_{xxx}^{eee}$ | YES | 1 | 1 |
| $A_{xxy}^{eem}$ | YES | –0.003 | 0.003 |
| $A_{yxx}^{mee}$ | YES | –0.0017 | 0.0017 |
| $A_{xyy}^{eee}$ | YES | 0.3126-0.114i | 0.3327 |
| $A_{xyx}^{eem}$ | YES | 0.0094-0.0153i | 0.018 |
| $A_{yyy}^{mee}$ | YES | –0.0074 + 0.0133i | 0.0153 |
| $A_{xxy}^{eee}$ | NO | 0.0084-0.002i | 0.0086 |
| $A_{xyy}^{eem} - A_{xxx}^{eem}$ | NO | –0.0349 + 0.0033i | 0.035 |
| $A_{yxy}^{mee}$ | NO | –0.0005 + 0.0038i | 0.0039 |

We have also compared the maximum signal level from the present sample to that from the lower-quality sample. After accounting for the different particle densities of the two samples, the SHG response of the present sample was found to be a factor of 10 higher. This enhancement arises from the narrower resonance and better resonance enhancement at the fundamental wavelength.

In conclusion, we have shown that improvements in sample quality, obtained by state-of-the-art nanofabrication, lead to significant advances in their effective nonlinear optical properties. In particular, the symmetry rules for second-harmonic generation are well fulfilled and the higher-multipole effects, which have been associated with defects, are almost completely suppressed. Furthermore, the efficiency of second-harmonic radiation is enhanced by a factor of 10 compared to similar samples of earlier generation. We have thus reached, to a very good approximation, the desired dipole limit where the nonlinear response arises from the overall structural features of the sample and is not significantly influenced by random defects. This result is an essential prerequisite for designing nonlinear metamaterials with engineered properties.

## Acknowledgments

This work was supported by the Academy of Finland (114913 and 132438). M. Z. acknowledges the Wihuri Foundation for financial support. The authors would like to thank Hannu Husu for fruitful discussions.

#157528 - $15.00 USD Received 2 Nov 2011; revised 7 Dec 2011; accepted 7 Dec 2011; published 15 Dec 2011